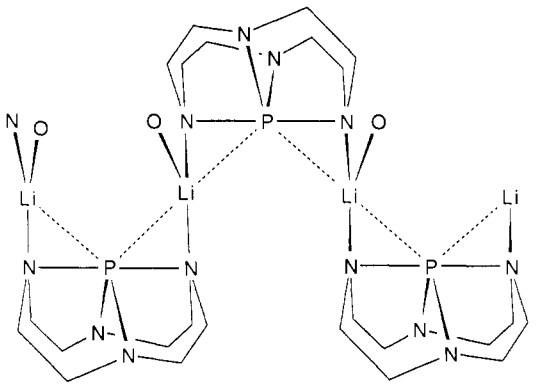

Figure 5. Illustration of $[Li(THF)cyclenP]_x$ (**7**) showing the Li---P interaction. Methylene groups of THF are omitted for clarity.

stabilized transition state involving cleavage of both axial bonds resulting in a phosphenium ion, not a phosphine.

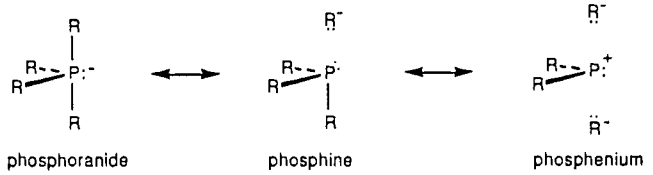

In light of the geometry of **7**, it appears that all three resonance forms are important in describing the electronics of phosphoranides, with the dominant form being dictated by the specific ligand set around the phosphorus atom.

The lithium geometry is approximately trigonal planar, considering the bonds to oxygen and nitrogen. The Li–O bond lengths are typical for Li–THF bonds, while the Li–N bonds are about 0.1 Å shorter than in usual $R_3N \rightarrow Li$ linkages.[19,20] The Li–N bond lengths are closer to amide–Li bond lengths (ca. 2.0 Å),[20,21] again reflecting the strong nucleophilic character of the axial nitrogens. Although the axial nitrogens are four-coordinate, the average P–N–Li angle is only 94°. This value can be compared to the close to tetrahedral P–N–B angle of 111° in **9**. The small angle may be due to a secondary interaction of the lithium with the lone pairs on the phosphorus atoms. The average Li–P distance in **7** of 2.92 Å is outside the usual range of directly bonded Li–P atoms in lithium diorganophosphides (about 2.4–2.7 Å)[22] but well within the range for a weak bonding interaction extended over the chain as depicted in Figure 5. In this way, each lithium bonds to two phosphorus atoms and each phosphorus to two lithiums. The P–M–N (M = metal) triangular bonding arrangement that results is quite common in cyclenPX derivatives (see **2–4**, above). This interaction may be primarily covalent, involving overlap of the empty 2p orbital on lithium with the phosphorus lone pair, or ionic, where electrostatic factors predominate.[20]

Acknowledgment. We thank the Robert A. Welch Foundation (M.L.) and National Science Foundation (P.P.P.) for generous financial support. M.L. thanks Fred Davidson for obtaining the NMR spectra.

Supplementary Material Available: Tables of anisotropic thermal parameters for **1** (X-ray), bond distances, bond angles, and hydrogen atom coordinates for **7**, a stereoview of **7** showing the packing, tables of camera distances and weighting functions, interatomic distances and amplitudes of vibration, a least-squares correlation matrix, and atomic coordinates, and molecular structure figures for **1** (electron diffraction) (12 pages); tables of observed and calculated structure factors for **1** and **7** (30 pages). Ordering information is given on any current masthead page.

(19) For example, N–Li bond lengths range from about 2.1 to 2.2 Å in Li(TMEDA) (TMEDA = tetramethylethylenediamine) complexes (see ref 20).
(20) Setzer, W. N.; Schleyer, P. v. R. *Adv. Organomet. Chem.* **1985**, *24*, 353.
(21) (a) Barr, D.; Clegg, W.; Mulvey, R. E.; Snaith, R. *J. Chem. Soc., Chem. Commun.* **1984**, 469. (b) Power, P. P.; Xiaojie, X. *J. Chem. Soc., Chem. Commun.* **1984**, 358. (c) Lappert, M. F.; Slade, M. J.; Singh, A.; Atwood, J. L.; Rogers, R. D.; Shakir, R. *J. Am. Chem. Soc.* **1983**, *105*, 302. (d) Barr, D.; Clegg, W.; Mulvey, R. E.; Snaith, R. *J. Chem. Soc., Chem. Commun.* **1984**, 285. (e) Engelhardt, L. M.; May, A. S.; Raston, C. L.; White, A. H. *J. Chem. Soc., Chem. Commun.* **1983**, 1671. (f) Rogers, R. D.; Atwood, J. L.; Gruning, R. *J. Organomet. Chem.* **1978**, *157*, 229.
(22) (a) Hey, E.; Hitchcock, P. B.; Lappert, M. F.; Rai, A. D. *J. Organomet. Chem.* **1987**, *325*, 1. (b) Hitchcock, P. B.; Lappert, M. F.; Power, P. P.; Smith, S. *J. Chem. Soc., Chem. Commun.* **1984**, 1669. (c) Jones, R. A.; Stuart, A. L.; Wright, T. C. *J. Am. Chem. Soc.* **1983**, *105*, 7459. (d) Hope, H.; Olmstead, M. M.; Xu, X.; Power, P. P. *J. Am. Chem. Soc.* **1984**, *106*, 819. (e) Bartlett, R. A.; Olmstead, M. M.; Power, P. P. *Inorg. Chem.* **1986**, *25*, 1243.

Contribution from the Laboratoire de Chimie de la Matière Condensée (UA 302, CNRS) and Laboratoire de Chimie Organique Industrielle (UA 403, CNRS), Ecole Nationale Supérieure de Chimie, 11 rue P. et M. Curie, 75005 Paris, France

EPR, ENDOR, and Optical Absorption Studies on the Electrochemically Produced Cycloheptatrienylcyclopentadienyltitanium $[(\eta^5\text{-}C_5H_5)Ti(\eta^7\text{-}C_7H_7)]$ Anion Radical

Didier Gourier[†] and Edmond Samuel*[,‡]

Received November 20, 1987

Cycloheptatrienylcyclopentadienyltitanium $[(\eta^5\text{-}C_5H_5)Ti(\eta^7\text{-}C_7H_7)]$ exhibits by cyclic voltammetry in THF a one-electron reversible reduction wave at −2.0 V (vs Ag/AgCl/KCl). The 17-electron paramagnetic radical anion produced, $[(\eta^5\text{-}C_5H_5)Ti(\eta^7\text{-}C_7H_7)]^-$, was fully characterized by EPR, and the magnetic parameters were determined by studies on liquid and frozen solutions. The optical spectra of both the neutral compound and the anion were measured and interpreted according to a molecular orbital scheme. The structure of the radical anion was determined by proton ENDOR at 30 and 100 K whereby it is shown that the geometry of the parent neutral molecule is preserved upon this one-electron reduction.

Introduction

Electron transfer in sandwich π complexes is a subject of continuing investigations, and of particular interest are simple systems such as the widely studied ferrocene/ferrocenium couple, in which this process occurs reversibly.

In the case of group 4 transition metals, the mixed-sandwich compounds are structural analogues of ferrocene and are therefore expected to undergo similar electron-transfer reactions. Nonetheless, this aspect of their chemistry seems to be very poorly documented. For this reason we undertook the following study on the diamagnetic 16-electron cyclopentadienylcycloheptatrienyltitanium compound, $[(\eta^5\text{-}C_5H_5)Ti(\eta^7\text{-}C_7H_7)]$, and the

[†] Laboratoire de Chimie de la Matière Condensée.
[‡] Laboratoire de Chimie Organique Industrielle.

0020-1669/88/1327-3018$01.50/0

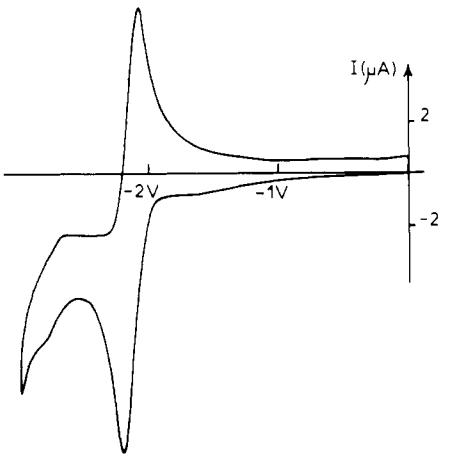

Figure 1. Cyclic voltammogram of [CpTi(cht)] in THF at −20 °C (scan speed 200 mV/s).

corresponding radical anion, hitherto unknown.

This compound was synthesized as early as 1970,[1] and the pseudosandwich structure was established by X-ray diffraction.[2] Later, molecular orbital calculations[3,4] and photoelectron studies[5,6] were employed to determine the electronic structure and charge distribution, subsequently supported by some experimental investigations such as nucleophilic substitutions[7,8] etc. We report herein our results on the electrochemistry of this compound, accompanied by EPR and also ENDOR on frozen solutions of the paramagnetic compound produced by one-electron reduction. We have shown previously[9] that, for $[(\eta^5\text{-}C_5H_5)Ti(\eta^8\text{-}C_8H_8)]$, ENDOR is a powerful tool in deriving structural information such as metal–proton distances in close agreement with X-ray diffraction methods (which give metal–carbon distances, the metal–proton distances then being calculated by taking a classical C–H bond length of 1.08 Å). This allowed us to make a direct structural comparison between the neutral and the anionic compounds studied.

Experimental Section

All manipulations were conducted under an inert atmosphere. [CpTi(cht)] was prepared by literature methods.[1] THF was used as solvent for electrochemical experiments. It was thoroughly dried and distilled over Na–benzophenone and then $LiAlH_4$ before use. The procedure for generating radicals in situ with an EPR–electrochemical cell and the instrument used for cyclic voltammetry experiments were described earlier.[10] Solution samples for ENDOR and UV–visible spectral measurements were produced by electrolysis under constant current in a cell provided with a platinum gauze for the anode, the cathodic cell consisting of a silver wire immersed in a suspension of KCl in the electrolytic solution. The electrolyzed solutions were then transferred under argon into the measurement cells. The EPR signal produced under these conditions was always of lower intensity compared to that generated by in situ electrolysis, but this handling was unavoidable for the purposes of ENDOR and optical absorption measurements. C_5D_6 was prepared according to the literature[11] and was used to prepare $[(\eta^5\text{-}C_5D_5)Ti(cht)]$ according to the regular procedure. EPR and ENDOR spectra were recorded with the same instruments and under the same conditions as previously described.[9] Optical absorption measurements were performed at room temperature with a Uvikon 860 spectrometer from Kontron Instruments.

Abbreviations used in this paper: Cp = $\eta^5\text{-}C_5H_5$; cht = $\eta^7\text{-}C_7H_7$; Me = CH_3; cot = $\eta^8\text{-}C_8H_8$.

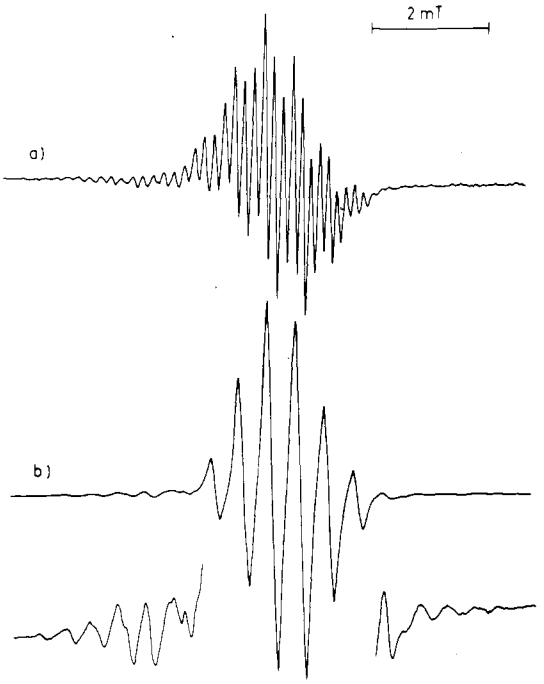

Figure 2. EPR spectra at room temperature of (a) $[CpTi(cht)]^-$ and (b) $[(\eta^5\text{-}C_5D_5)Ti(cht)]^-$ radical anions in THF generated in situ by electrolysis in the spectrometer cavity (current intensity 50 μA).

Cyclic Voltammetry and Electron Paramagnetic Resonance

[CpTi(cht)] exhibits by cyclic voltammetry in THF a one-electron reduction wave at −2 V (Figure 1). Repeated measurements at scan speeds from 100 to 500 mV/s show that this wave is reversible. The CV experiments are best performed at −20 °C due to the instability of the anionic species, which decomposes at room temperature. The identity of the reduced species as being the expected 17-electron anion was clearly established by electrolysis in the EPR cavity.

Figure 2a shows the EPR spectrum of the $[CpTi(cht)]^-$ radical, recorded at room temperature. It is attributed to an unpaired electron spin $S = {}^1/_2$ interacting with proton nuclei of the Cp and cht rings. The weak transitions at low magnetic fields are due to hyperfine interaction with ^{47}Ti ($I = {}^5/_2$, abundance 7.75%) and ^{49}Ti ($I = {}^7/_2$, abundance 5.51%) nuclei; the corresponding transitions at high field are too broad to be detectable. From the crowded spectrum, it is difficult to extract magnetic parameters with sufficient accuracy; the EPR spectrum can be significantly simplified by deuteriating the Cp ligand. The EPR spectrum of $[(\eta^5\text{-}C_5D_5)Ti(cht)]^-$ depicted in Figure 2b is composed of a set of eight lines with intensities 1:7:21:35:35:21:7:1 due to the hyperfine interaction of the electron spin with the seven equivalent protons of the cht ring. From the two spectra of Figure 2, the isotropic g and proton hyperfine parameters are $g_{iso} = 1.986$ (9), $A_{iso}(cht) = +13$ MHz, and $A_{iso}(Cp) = +4$ MHz. The sign of the hyperfine interactions is taken as positive, consistent with the assignment found in other sandwich compounds.[12] The decrease of spectral density induced by deuteriation of the Cp ring allows one to determine the isotropic titanium coupling constant $\langle A^{Ti} \rangle = 24$ MHz. The high-field hyperfine lines are broadened, as is frequently found in other organometallic compounds. This effect arises from modulation of the **g** and hyperfine tensors due to molecular tumbling motion.[13]

(1) Van Oven, H. O.; De Liefde Meijer, H. J. *J. Organomet. Chem.* **1970**, *23*, 159.
(2) Zeinstra, J. D.; de Boer, J. L. *J. Organomet. Chem.* **1973**, *54*, 207.
(3) Clack, D.; Warren, D. *Theor. Chim. Acta* **1977**, *46*, 313.
(4) Zeinstra, J. D.; Nieupoort, W. C. *Inorg. Chim. Acta* **1978**, *30*, 103.
(5) Evans, S.; Green, J. C.; Jackson, S. E. *J. Chem. Soc., Dalton Trans.* **1973**, 304.
(6) Andréa, R. R.; Terpstra, A.; Oskam, A.; Bruin, P.; Teuben, J. H. *J. Organomet. Chem.* **1986**, *307*, 307.
(7) Groenboom, C. J.; de Liefde Meijer, H. J.; Jellinek, F. *Recl. Trav. Chim. Pays-Bas* **1974**, *93*, 6.
(8) Groenboom, C. J.; de Liefde Meijer, H. J.; Jellinek, F. *J. Organomet. Chem.* **1974**, *69*, 235.
(9) Gourier, D.; Samuel, E. *J. Am. Chem. Soc.* **1987**, *109*, 4571.
(10) Samuel, E.; Guery, D.; Vedel, J.; Basile, F. *Organometallics* **1985**, *4*, 1073.
(11) Anderson, G. K.; Cross, R. J.; Phillips, G. I. *J. Chem. Soc., Chem. Commun.* **1978**, 709.
(12) Wolf, R.; Schweiger, A.; Gunthard, H. *Mol. Phys.* **1984**, *53*, 567.

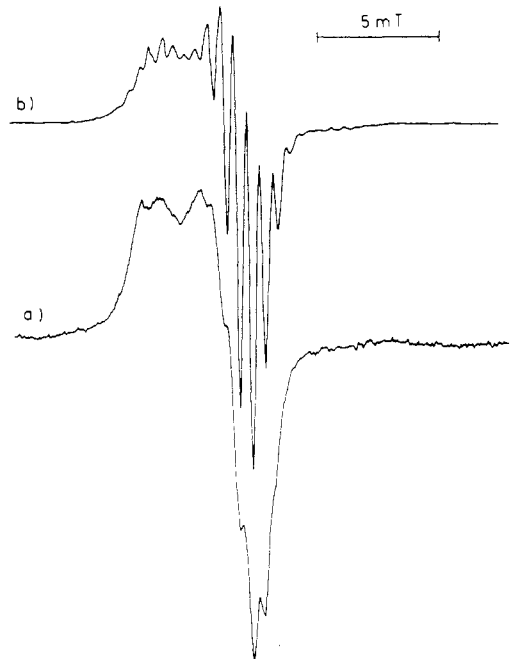

Figure 3. EPR spectra at 130 K of (a) $[CpTi(cht)]^-$ and (b) $[(\eta^5\text{-}C_5D_5)Ti(cht)]^-$ radical anions generated in situ by electrolysis in the spectrometer cavity (current intensity 50 μA).

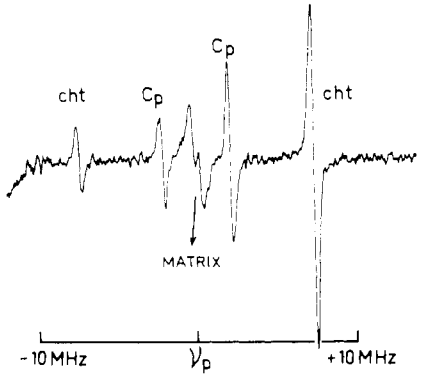

Figure 4. Proton ENDOR spectrum of $[CpTi(cht)]^-$ recorded at 100 K (microwave power 40 mW, radio-frequency power 100 W). The rf field is modulated at 12.5 kHz with a modulation depth of +100 kHz (sweep time 200 s). The magnetic field is set at 343.6 mT.

The EPR spectra in frozen solution at 130 K are shown in Figure 3. They reveal the axial symmetry of the **g** tensor, with principal values $g_\parallel = 1.999$ (9) and $g_\perp = 1.980$ (4). The structure detectable on the perpendicular part of the spectrum in Figure 3a is due to a partially resolved hyperfine interaction with ring protons. The spectrum is better resolved in the compound deuteriated on the Cp ring (Figure 3b), where two components of the hyperfine interaction with cht protons can be measured, $\langle A_\parallel \rangle = 12$ MHz and $\langle A_\perp \rangle = 15$ MHz. It should be pointed out, however, that these values are not the principal values of the proton hyperfine tensor, since at 130 K, the rings are rapidly reorienting and the hyperfine interaction is motionally averaged.[9] This is the reason the hyperfine parameters are inserted in brackets.

Proton ENDOR

Typical ENDOR spectra recorded at 100 and 30 K are shown in Figures 4 and 5. They were both obtained by saturating the powder EPR spectrum at about 344 mT. At 100 K, the ENDOR spectrum is single crystal like and is composed of four narrow and symmetrical lines corresponding to the interaction with the ring protons, the signal at the proton frequency resulting from the interaction with nearby protons of solvent molecules (matrix

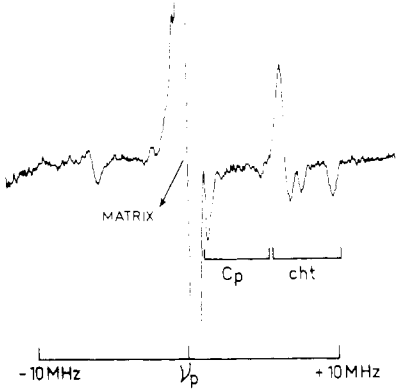

Figure 5. Proton ENDOR spectrum of $[CpTi(cht)]^-$ recorded at 30 K (microwave power 3.1 mW, radio-frequency power 100 W). The rf field is modulated at 12.5 kHz with a modulation depth of +150 kHz (sweep time 200 s). The magnetic field is set at 343.8 mT.

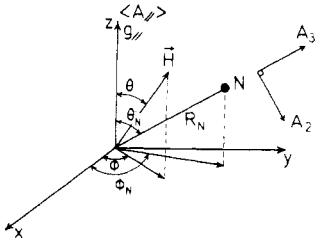

Figure 6. Coordinate system used for ENDOR experiments. Each ring proton is at a distance R_N from Ti and makes angles θ_N and ϕ_N with the molecular axis (z axis) and the x axis. The magnetic field makes angles θ and ϕ with these axes. Also represented are the directions of the two principal axes A_3 and A_2 of the proton hyperfine tensor. The A_1 axis is perpendicular to the figure and thus parallel to the ring planes.

ENDOR). At 30 K, the spectrum is composed of a strong matrix line superimposed on weak, broad, and powderlike ENDOR lines representing the interaction with ring protons. These two very different line shapes result from different regimes of the ring motion. To visualize this effect, let us consider a given proton (labeled N) of one ring, at a distance R_N from the Ti atom, making an angle θ_N with the molecular axis (z axis) and an angle ϕ_N with the x direction (Figure 6). The corresponding hyperfine parameters are A_i ($i = 1, 2, 3$) with the A_3 axis lying along the titanium–proton direction. Such a coincidence between the A_3 axis and the metal–proton direction is likely to occur since the anisotropic part of the hyperfine interaction is almost purely of a point dipole–dipole nature and also because in our case the metal–proton distance is larger than 2 Å. The Cp and cht rings can undergo uniaxial reorientations around the molecular axis.[9] If the motion is slow compared to the time scale of the ENDOR experiment, which is of the order of the anisotropy of the hyperfine coupling in the xy plane, the proton can be considered as fixed. If the magnetic field H is parallel to the titanium–proton direction, the ENDOR spectrum is composed of two lines at frequencies $\nu(m_s) = \nu_p \pm A_3/2$. However, if the magnetic field orientation is characterized by angles θ and ϕ with the z and x axes, we expect two ENDOR transitions at frequencies[14]

$$\nu(m_s) = \left[\sum_{i=1}^{3} \left(\frac{m_s}{g} g_i A_i h_i - h_i \nu_p \right)^2 \right]^{1/2} \quad (1)$$

with

$$g^2 = \sum_{i=1}^{3} h_i^2 g_i^2$$

where h_i is the direction cosine between the magnetic field and the ith hyperfine tensor axis.

(13) Rogers, R N.; Pake, G. E. *J. Chem. Phys.* **1960**, *33*, 1107.

(14) Hurst, G. L.; Henderson, T. A.; Kreilick, R. W. *J. Am. Chem. Soc.* **1985**, *107*, 7294.

Table I. EPR and ENDOR Parameters of the [CpTi(cht)]$^-$ Radical Anion[a]

		ENDOR	EPR
	$g_\parallel$		1.999 (9)
	$g_\perp$		1.980 (4)
Ti	$\langle A \rangle$		+24
cht protons	$\langle A_\parallel \rangle$	+13.2 (2)	+12
	$\langle A_\perp \rangle$	+14.6 (7)	+15
	A_{iso}	+14.1 (9)	+13
	A_3	+18.8 (0)	
	A_2	+12.0 (0)	
	A_1	+11.7 (7)	
Cp protons	$\langle A_\parallel \rangle$	+5.4 (0)	
	$\langle A_\perp \rangle$	+3.9 (1)	
	A_{iso}	+4.4 (1)	+4
	A_3	+9.6 ± 0.1	
	A_2	+1.8 ± 0.1	
	A_1	+1.8 ± 0.1	

[a] Hyperfine interactions are given in MHz.

In frozen solution, the ENDOR spectrum is obtained by saturating the EPR spectrum at a resonant field H_0, corresponding to the selection of a given set of molecular orientations.[15,16] If the **g** tensor is axial, the magnetic field setting H_0 implies the selection of molecules with their axes making an angle θ with H. However, the angle ϕ can assume all the possible values between 0 and 360°. The resulting ENDOR spectrum is thus an average of all the values of ϕ and exhibits a powder shape with two or three peaks for each m_s state,[16] due to a slower variation of the ENDOR frequency with ϕ. Such a powder ENDOR spectrum, characteristic of a slow ring reorientation, was obtained at 30 K as shown in Figure 5.

If the ring motion around the molecular axis is rapid compared to the ENDOR time scale, the hyperfine interaction with the proton is averaged and the principal axis of the hyperfine tensor is now parallel to the molecular axis instead of the metal–proton direction. Since the averaged hyperfine tensor and the **g** tensor are axial and collinear, all the molecules selected by the magnetic setting H_0 exhibit the same ENDOR spectrum, which is now single crystal like.[16] The spectrum recorded at 100 K (Figure 4) is thus characteristic of a fast ring reorientation. In this case, expression 1 giving the ENDOR frequencies becomes

$$\nu(m_s) = \left[\left(\frac{m_s}{g} g_\parallel \langle A_\parallel \rangle - \nu_p\right)^2 \cos^2\theta + \left(\frac{m_s}{g} g_\perp \langle A_\perp \rangle - \nu_p\right)^2 \sin^2\theta\right]^{1/2} \quad (2)$$

where $\langle A_\parallel \rangle$ and $\langle A_\perp \rangle$ are the two values for the averaged hyperfine tensor. This expression can be arranged to give a linear relation:

$$\left(\frac{\nu^2(-) - \nu^2(+)}{2\nu_p}\right) g = (g_\parallel \langle A_\parallel \rangle - g_\perp \langle A_\perp \rangle) \cos^2\theta + g_\perp \langle A_\perp \rangle \quad (3)$$

with

$$\cos^2\theta = (g^2 - g_\perp{}^2)/(g_\parallel{}^2 - g_\perp{}^2)$$

where the signs + and − represent the m_s states $\pm^1/_2$.

For different magnetic field settings $[\nu^2(-) - \nu^2(+)]g/2\nu_p$ versus $(g^2 - g_\perp{}^2)/(g_\parallel{}^2 - g_\perp{}^2)$ was plotted and the values of the hyperfine parameters $\langle A_\parallel \rangle$ and $\langle A_\perp \rangle$ for the two rings were obtained by a least-squares fit of the data (Figure 7). The proton hyperfine parameters $\langle A_\parallel \rangle$ and $\langle A_\perp \rangle$ deduced from these plots and the isotropic hyperfine interaction A_{iso} are given in Table I. A_{iso} is related to $\langle A_\parallel \rangle$ and $\langle A_\perp \rangle$ by

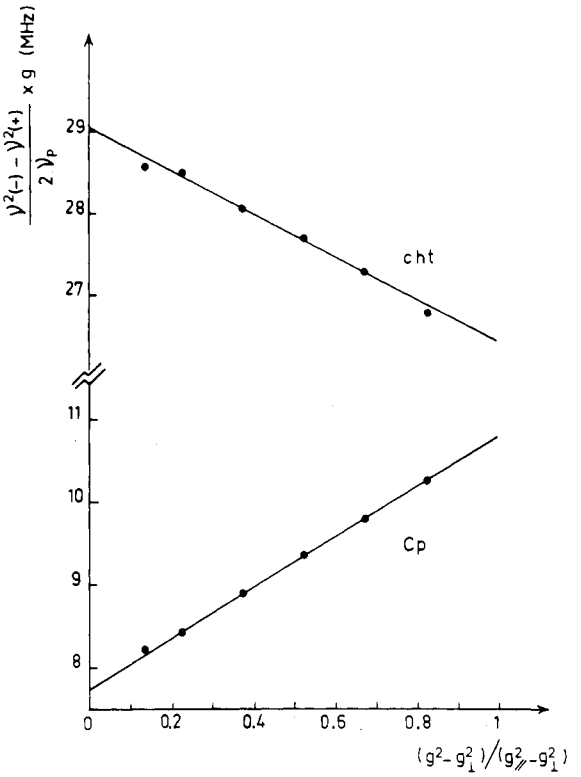

Figure 7. Plots of $[\nu^2(-) - \nu^2(+)]g/2\nu_p$ versus $(g^2 - g_\perp{}^2)/(g_\parallel{}^2 - g_\perp{}^2)$ for Cp and cht protons of [CpTi(cht)]$^-$ at 100 K. + and − signs represent the $m_s = +^1/_2$ and $-^1/_2$ states, respectively.

$$A_{iso} = \frac{1}{3}(\langle A_\parallel \rangle + 2\langle A_\perp \rangle) \quad (4)$$

The signs of the hyperfine parameters must be positive in order to obtain A_{iso} values consistent with the EPR results. Other combinations of signs for $\langle A_\parallel \rangle$ and $\langle A_\perp \rangle$ would give anomalously small values of A_{iso}. It should be noticed that the isotropic hyperfine interaction found for Cp protons is very similar to the value +4.09 MHz found for these protons in [CpTi(cot)] and that the value A_{iso} = +14.1 (9) MHz for cht protons is significantly larger than A_{iso} = +8.78 MHz found for cot protons in the same compound.[9]

The ENDOR spectra recorded at 30 K in the regime of slow ring motion allow one to measure the principal values A_i (i = 1, 2, 3) of the proton hyperfine coupling. However, the spectra are now powderlike because there is a finite angle θ_N between the A_3 axis of the hyperfine interactions and the $g_\parallel$ axis and it is thus not possible to interpret the data by plots such as those used at 100 K in the rapid-motion regime. The proton hyperfine tensor is composed of the isotropic part A_{iso} and the traceless dipolar part A_i^{dip}:

$$A_i = A_{iso} + A_i^{dip} \quad (5)$$

$$A_{iso} = {}^1/_3 \sum_{i=1}^{3} A_i$$

A_{iso} is known from the spectra recorded at 100 K; thus, measurement of two components for each kind of protons is necessary to get the whole hyperfine interaction. Since A_{iso} and $A_3{}^{dip}$ are positive, the component A_3(cht) should be positive and larger than 14 MHz. Stepwise variations of the magnetic field setting H_0 in the EPR spectrum result in shifts of the ENDOR frequencies, and for the special case where H_0 corresponds to a selected angle θ close to θ_N for cht protons, one ENDOR line reaches its maximum shift from the proton frequency. This line is thus at the frequency $\nu_3 = \nu_p + A_3(\text{cht})/2$, and we obtained A_3(cht) = +18.8 (0) MHz; the two other components A_1(cht) and A_2(cht) are thus

(15) Rist, G. H.; Nyde, J. S. *J. Chem. Phys.* **1970**, *52*, 4633.
(16) Hoffman, B. M.; Martinsen, J.; Venters, R. A. *J. Magn. Reson.* **1984**, *59*, 110.

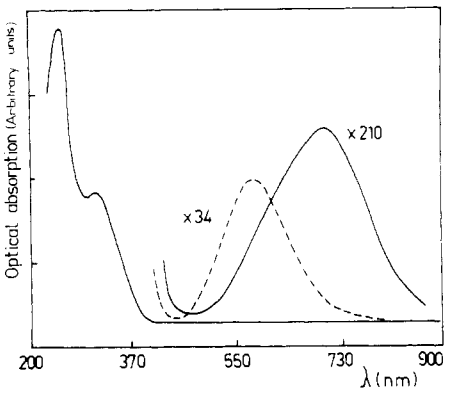

Figure 8. Optical absorption spectra of neutral [CpTi(cht)] (full line) and $[CpTi(cht)]^-$ radical anion (dashed line) recorded at room temperature in THF. The extinction coefficients ϵ for the bands at 697.5 and 597 nm are 24 and 140, respectively.

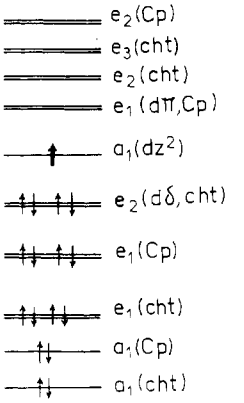

Figure 9. Schematic energy level diagram (not to scale) of [CpTi(cht)], involving the 3d metal orbitals and the π orbitals of the Cp and cht rings. Orbital occupancy in the neutral compound is represented by full arrows, while the additional electron in the radical anion is represented by a bold arrow.

on the order of +12 MHz. Furthermore, one of the hyperfine tensor axes (A_1 axis) being parallel to the ring planes,[12] the corresponding hyperfine value can be measured by setting H_0 at the high-field flank of the EPR spectrum, corresponding to the selected angle $\theta = \pi/2$. We obtained $A_1(cht) = +12.0$ (0) MHz, and the third hyperfine component $A_2(cht) = +11.7$ (7) MHz is deduced from A_{iso}, $A_3(cht)$, and $A_1(cht)$. In principle, the same procedure can be used for Cp protons. However, the stepwise variations of H_0 showed that the ENDOR line at frequency $\nu_3 = \nu_p + A_3(Cp)/2$ is hindered at the flank of the low-frequency ENDOR line of cht protons. The high-frequency ENDOR line of Cp protons [$\nu_{max}(Cp)$] is only detectable when H_0 is such that θ deviates significantly from θ_N. The variation of $\nu_{max}(Cp)$ with H_0 allowed us to estimate $A_3(Cp)$ to be about $+9.6 \pm 0.1$ MHz. From the ENDOR line near the strong matrix ENDOR line, we deduced $A_1(Cp) = A_2(Cp) = +1.8 \pm 0.1$ MHz. Although these values are not precise, they are comparable to $A_3(Cp) = +9.3$ MHz, $A_1(Cp) = +1.5$ MHz, and $A_2(Cp) = +1.4$ MHz observed for [CpTi(cot)].[9] All the ENDOR results for $[CpTi(cht)]^-$ are gathered in Table I.

Optical Absorption

The optical absorption (OA) spectra of [CpTi(cht)] and the $[CpTi(cht)]^-$ radical in THF are shown in Figure 8. The neutral compound in dilute THF solution is pale blue and exhibits a band at 697.5 nm (1.78 eV, $\epsilon = 24$) and two strong bands at 252 nm (4.92 eV, $\epsilon = 11\,000$) and 313 nm (3.96 eV, $\epsilon = 3000$). Since the ground-state configuration of [CpTi(cht)] is $e_1^4e_2^4$ (Figure 9), the band at low photon energy is due to the excitation of one e_2 electron to the low-lying a_1 orbital, i.e.

$$^1A_1(e_1^4e_2^4) \rightarrow {}^1E_2(e_1^4e_2^3a_1)$$

The e_2 and a_1 orbitals having respectively ~41% and 97% metal character,[4] this transition is thus partly d–d and partly ligand (cht) to metal charge transfer. The electrochemical reduction of [CpTi(cht)] yields a deep violet solution with a shift of the low-energy band to 579 nm (2.14 eV) and a significant increase of its intensity ($\epsilon = 140$). In order to be sure that this band is not due to a decomposition product, we have recorded the OA spectrum of the compound [CpV(cht)], whose ground state $^2A_1(e_2^4a_1)$ is the same as that expected for $[CpTi(cht)]^-$. It exhibits a band at 563.0 nm (2.20 eV) very similar in shape to the 579-nm band of $[CpTi(cht)]^-$.

This absorption can be attributed to the spin-allowed transitions

$$^2A_1(e_2^4a_1) \rightarrow {}^2E_1(e_2^4e_1)$$

$$^2A_1(e_2^4a_1) \rightarrow {}^2E_2(e_2^3a_1^2)$$

MO calculations in [CpV(cht)] predict that they should occur at about the same photon energy, $\simeq 1.9$ and 2.1 eV, respectively.[3] The "Laporte" selection rule is relaxed in this case because titanium lies in a field having no inversion symmetry. However, the $^2A_1 \rightarrow {}^2E_2$ transition is forbidden in both C_5 and C_7 symmetries, although the $^2A_1 \rightarrow {}^2E_1$ transition is allowed in these symmetries if the electric field is perpendicular to the molecular axis. Thus, the low-energy transition in neutral [CpTi(cht)] is symmetry-forbidden, and the significant increase of this band upon reduction can be explained if it is attributed to the $^2A_1 \rightarrow {}^2E_1$ transition in $[CpTi(cht)]^-$. Since the e_1 orbital has a metal character of about 75%, this transition is mainly a d–d transition, with a small metal to ligand (Cp) charge-transfer character.

Discussion

Formally Ti can be considered in [CpTi(cht)] as a $Ti^0(d^4)$ atom surrounded by one Cp^- and one cht^+ ion. Although the σ orbitals of the rings are involved in the metal–ring bonding, especially with the metal 4s and 4p orbitals, the dominant contribution arises from the interaction between the metal 3d orbitals and the π system of the rings.[3] Figure 9 shows a schematic energy level diagram of a [CpTi(cht)] complex. Ti–Cp and Ti–cht bonds differ characteristically. The first one is almost exclusively a π-type bond, and the negative charges on the Cp carbons become positive due to π-electron donation to the $3d\pi$ (d_{xz}, d_{yz}) metal orbitals, through bonding with the filled $e_1(Cp)$ orbitals. In contrast a significant amount of electronic charge is drained from the metal into the cht ring by considerable back-bonding interaction of the $3d\delta$ ($d_{x^2-y^2}$, d_{xy}) metal orbitals with the vacant $e_2(cht)$ orbitals. Thus, electrons are effectively channeled from the formally negatively charged Cp ring onto the positively charged cht ring via the metal. The effective charges of Cp, cht, and Ti are now −0.7, −1.0, and +1.7, respectively.[4] The cht ring is bound more strongly to the metal than the Cp ring, which explains the shorter metal–carbon distance of the Ti–C(cht) bond, compared with the Ti–C(Cp) bond[2] (respectively 2.19 and 2.32 Å). The nonbonding a_1 orbital is essentially the d_{z^2} metal orbital, with a small 4s character. The electronic ground state of [CpTi(cht)] is $^1A_1(e_2^4)$, and we thus expect that the anion $[CpTi(cht)]^-$ formed upon reduction adopts a $^2A_1(e_2^4a_1)$ ground state. In principle, occupancy of the nonbonding a_1 orbital should not modify the bonding properties of the complex.

EPR and ENDOR parameters measured in $[CpTi(cht)]^-$ allow one to probe both the electronic ground state and the structure of this compound. The deviation of the g factor from its free electron spin value $g_e = 2.0023$ being due to a spin–orbit admixture of excited electronic states into the ground state, the absence of g shift observed when the magnetic field is parallel to the molecular axis ($g_\parallel = 1.999$ (9)) shows that the unpaired spin lies in a metal orbital with predominantly d_{z^2} character, for which the g values are predicted to be

$$g_\parallel = 2.0023$$

$$g_\perp = 2.0023 - \frac{6\lambda_{eff}}{E_{d_z} - E_{d_{xy},d_{yz}}} \qquad (6)$$

Table II. Titanium–Proton Distance R_N and Angle θ_N between the Molecular Axis and the Titanium–Proton Direction in [CpTi(cht)] and [CpTi(cht)]$^-$ Compounds

		[CpTi(cht)] X-ray data[a]	[CpTi(cht)]$^-$ ENDOR data
Cp	R_N, Å	3.0	3.1
	θ_N, deg	49	47
cht	R_N, Å	3.1	3.3
	θ_N, deg	61	65

[a] Data calculated on the basis of metal–carbon distances taken from ref 2 by assuming a C–H bond length of 1.08 Å.

where λ_{eff} is the effective spin–orbit coupling constant. Our results confirm that the electronic ground state of [CpTi(cht)]$^-$ is $^2A_1(e_2^4a_1)$, as predicted from MO calculation.[3,4]

We may estimate λ_{eff} using $g_\perp$ and the energy of the optical absorption $^2A_1(e_2^4a_1) \rightarrow {}^2E_1(e_2^4e_1)$ at 2.14 eV since this transition involves the a_1 orbital of d_{z^2} character and the e_1 orbital of d_{xz}, d_{yz} character. λ_{eff} is found to be 63 cm^{-1}, a value lower than λ = 155 cm^{-1} expected for a free Ti^{3+} ion, which points to the existence of a low charge on the metal atom. The λ_{eff} value found in [CpTi(cht)]$^-$ is close to λ = 71 cm^{-1} found for Ti with zero charge.[17] MO calculations and ESCA measurements on the neutral compound [CpTi(cht)] gave respectively charges of +1.7 and +1.1 on the Ti atom. Since the a_1 orbital is of almost purely metal character, the additional electron in the anion should thus be localized on the Ti atom and its charge should thus be reduced to +0.7 or +0.1, in good agreement with that deduced from the low effective spin–orbit coupling constant.

The modification of the molecular structure brought about on passing from the neutral compound to the anion can be studied by using the proton hyperfine interaction parameters. The two important structural parameters obtained from ENDOR are the titanium–proton distance R_N and the angle θ_N between the molecular axis and the titanium–proton direction. The hyperfine tensors are almost axial for both Cp and cht protons, which confirms that A_{dip} is of purely dipole–dipole nature and that the A_3 axis is almost collinear with the titanium–proton direction. θ_N is thus simply the angle between the titanium–proton axis and the molecular axis, which is also the axis of ring reorientation.

The angle θ_N is thus related to the components of the motionally averaged hyperfine tensors and the components A_i (i = 1, 2, 3) of the hyperfine tensors in the static case by the expression

$$\theta_N = \cos^{-1}\left[\left(\frac{\langle A_\parallel\rangle - A_2}{A_3 - A_2}\right)^{1/2}\right]$$

or

$$\theta_N = \cos^{-1}\left[\left(\frac{2\langle A_\perp\rangle - A_1 - A_3}{A_2 - A_3}\right)^{1/2}\right] \quad (7)$$

Since the titanium–proton distance is higher than 2 Å, the following point dipole–dipole expression can be used for R_N:

$$R_N = \left(\frac{2g\beta g_N\beta_N}{A_3 - A_{iso}}\right)^{1/3} \quad (8)$$

The values of θ_N and R_N for [CpTi(cht)]$^-$ are gathered in Table II and compared with the corresponding parameters for [CpTi(cht)]. For the latter compound, the X-ray data give only titanium–carbon distances. R_N and θ_N are thus estimated by taking a C–H bond length of 1.08 Å. The two parameters are very similar in the neutral and the anionic complexes, and the small discrepancies may be due to experimental uncertainties. This similarity of structures in the two compounds confirms the essentially nonbonding character of the $a_1(d_{z^2})$ orbital, since the bond strength is not affected when this orbital is occupied by one electron.

The isotropic proton hyperfine parameter A_{iso} is related to the proton spin density ρ_H by the expression

$$A_{iso} = \frac{8\pi}{3}g\beta g_N\beta_N|\psi_0(s)|^2\rho_H \quad (9)$$

From the experimental results, we obtain $\rho_H(Cp) = +3.1 \times 10^{-3}$ and $\rho_H(cht) = +10.0 \times 10^{-3}$ for Cp and cht protons, respectively. The spin density on Cp protons is very similar to the value $\rho_H(Cp) = +2.9 \times 10^{-3}$ found in [CpTi(cot)], although the spin density on cht protons is larger than $\rho_H(cot) = +6.2 \times 10^{-3}$ found for cot protons.[9] This arises from a direct delocalization of the unpaired electron spin on the 1s hydrogen orbital. The experimental results point to a stronger Ti–H interaction with the cht ring than with the Cp and cot rings in [CpTi(cot)], as a consequence of the shorter Ti–cht distance compared with Ti–cot and Ti–Cp distances.

If we go back to the EPR spectrum, some characteristics of the titanium hyperfine interaction can be discussed, although the principal values $A_\parallel^{Ti}$ and $A_\perp^{Ti}$ of the hyperfine tensors could not be measured because of the poor spectral resolution. The averaged interaction $\langle A^{Ti}\rangle$ = +24 MHz measured in the liquid solution is related to the isotropic hyperfine coupling A_{iso} and to the perpendicular g shift $\Delta g_\perp = g_\perp - 2.0023$ by the expression

$$\langle A^{Ti}\rangle = A_{iso}^{Ti} + \frac{2P}{3}\Delta g_\perp \quad (10)$$

The parameter P being about −28 MHz for a titanium with zero charge,[18] the term $2P(\Delta g_\perp)/3$ is found to be 0.4 MHz and can be neglected. The isotropic hyperfine coupling A_{iso}^{Ti} = +24 MHz is significantly smaller than A_{iso}^{Ti} = +41 MHz found for [CpTi(cot)].[19] This points to a larger contribution of the metal 4s orbital to the a_1 ground-state MO in [CpTi(cht)]. Assuming a spin density of 1 unit at the metal, A_{iso} is composed of two contributions of opposite signs

$$A_{iso}^{Ti} = \chi[A_{iso}^{Ti}(d_{z^2})] + (1 - \chi)[A_{iso}^{Ti}(4s)] \quad (11)$$

where χ and $1 - \chi$ are the spin densities in the d_{z^2} and 4s orbitals, respectively. $1 - \chi$ is small, generally on the order of 10^{-2}. $A_{iso}^{Ti}(d_{z^2})$ and $A_{iso}^{Ti}(4s)$ are respectively the positive contributions of spin polarization of inner ns (n = 1, 2, 3) orbitals and the negative direct contribution of the partially occupied 4s orbital. Since $A_{iso}^{Ti}(4s)$ is large and negative ($A_{iso}^{Ti}(4s)$ = −492 MHz), a small increase of the 4s contribution to the ground state can significantly decrease A_{iso}^{Ti}.

Concluding Remarks

The present study by EPR and ENDOR on the electrochemically produced [CpTi(cht)]$^-$ radical anion fully supports the predictions derived from MO calculations on neutral [CpTi(cht)]. It also confirms that reliable structural information can be obtained from ENDOR frozen solutions for this family of pseudoaxial complexes, although it was postulated that such structural information could only be obtained by dilution in a diamagnetic isostructural monocrystalline host.[21] In the latter case the parameters are obtained with high accuracy, but the data are collected by crystal rotation inside the magnetic field in three orthogonal planes and treated with an elaborate mathematical arsenal. Owing to the simplicity in deriving the parameters with the ENDOR frozen-solution method, the small loss of precision compared to that of the single-crystal-phase method is not of such a dramatic importance if the purpose is to obtain information pertaining to chemical properties or reactivity such as nucleophilic substitution on the rings.

(17) Dunn, T. M. *Trans. Faraday Soc.* **1961**, *57*, 1441.
(18) McGarvey, B. R. *J. Phys. Chem.* **1967**, *71*, 51.
(19) Samuel, E.; Labauze, G.; Vivien, D. *J. Chem. Soc., Dalton Trans.* **1979**, 956.
(20) Elschenbroich, C.; Bilger, E.; Koch, J. *J. Am. Chem. Soc.* **1984**, *106*, 4297.
(21) Schweiger, A. *Struct. Bonding (Berlin)* **1982**, 51.

This method can also be particularly powerful in cases where the EPR spectrum is very poorly resolved and yields no information, as is the case with the neutral paramagnetic compound $[(\eta^5\text{-}C_5Me_5)Zr(cot)]$;[22] ENDOR then becomes valuable in supplying the desired information without necessarily resorting to X-ray diffraction methods. Proton and ^{91}Zr ENDOR studies on the latter compound are under way.

(22) Blenkers, J.; Bruin, P.; Teuben, J. H. *J. Organomet. Chem.* **1985**, *297*, 61.

Registry No. [CpTi(cht)], 51203-49-7; $[CpTi(cht)]^-$, 115338-78-8; $[(\eta^5\text{-}C_5D_5)Ti(cht)]$, 115338-79-9; $[(\eta^5\text{-}C_5D_5)Ti(cht)]^-$, 115338-80-2; THF, 109-99-9.

Contribution from the Department of Chemistry, Queen's University, Kingston, Canada K7L 3N6

Carbon Monoxide and Carbon Dioxide Hydrogenation Catalyzed by Supported Ruthenium Carbonyl Clusters. A Novel Procedure for Encapsulating $Ru_3(CO)_{12}$ within the Pores of Na-Y Zeolite

W. Ross Hastings, Charles J. Cameron, Marian J. Thomas, and Michael C. Baird*

Received December 23, 1987

Zeolite-supported ruthenium catalysts for the hydrogenation of carbon monoxide and carbon dioxide have been prepared by sorbing $Ru(CO)_5$ (molecular diameter 6.3 Å) onto Na-Y zeolite and Linde 5A molecular sieve. Although the metal carbonyl is not absorbed into the pores of the molecular sieve (diameter 4.2 Å), it is readily absorbed into the pores (diameter 7.4 Å) and supercages (diameter 13 Å) of the Na-Y zeolite. The $Ru(CO)_5$ in Na-Y converts in the absence of carbon monoxide to the much larger $Ru_3(CO)_{12}$ (diameter 9.2 Å), which remains on the surface of the molecular sieve but is trapped within the supercages of the Na-Y zeolite because it cannot pass through the smaller pores. Slow, temperature-programmed heating of the $Ru_3(CO)_{12}$ in Na-Y to 350 °C under a flow of hydrogen results in decarbonylation and formation of a CO hydrogenation catalyst that produces a very atypical (for ruthenium) hydrocarbon distribution truncated at about C_{10}. The unusual product distribution presumably arises because the catalyst sites are situated within the zeolite supercages. Thus the metal is highly dispersed and/or the growing hydrocarbon chains are subject to geometrical limitations on their growth. Consistent with this hypothesis, ruthenium carbonyl clusters immobilized on the external surfaces of Na-Y zeolite, Linde 5A molecular sieve, and γ-alumina all exhibit typical, nonselective hydrocarbon product distributions. The same supported ruthenium carbonyl clusters are also extremely active catalysts for the selective hydrogenation of CO_2 (H_2:CO_2 = 4:1) to methane. At a lower H_2:CO_2 ratio (1:1), however, Na-Y-supported $Ru_3(CO)_{12}$ catalyzes the hydrogenation of CO_2 to higher hydrocarbons as well (up to C_{16}). Interestingly, CO_2 hydrogenation differs from CO hydrogenation in that the former process (a) yields no olefins or isoalkanes, both of which are prominent from CO hydrogenation, and (b) does not result in a product distribution exhibiting the depletion in C_2 products normally obtained from CO hydrogenation. In spite of these apparently significant differences, it is argued that CO_2 hydrogenation involves initial reduction of the CO_2 to CO and that hydrogenation of both proceeds via the same carbidic mechanism proposed elsewhere.

In recent years, considerable research has been directed toward gaining a better understanding of reactions involving the ruthenium-catalyzed hydrogenation of carbon monoxide[1] and dioxide.[2] Catalysts formed by supporting both inorganic ruthenium salts[3] and ruthenium carbonyl clusters[2c,k,3g,h,4] on simple oxides have been shown to reduce CO to a wide variety of products, and there have also been a number of publications dealing with CO-hydrogenation catalysts containing ruthenium in zeolites and similar materials.[5] In contrast, the hydrogenation of CO_2 catalyzed by ruthenium

(1) For reviews, see: (a) Anderson, R. B. *The Fischer-Tropsch Synthesis*; Academic: New York, 1984. (b) King, F.; Shutt, E.; Thomson, A. I. *Platinum Met. Rev.* **1985**, *29*, 146.

(2) (a) Mill, G. A.; Steffgen, F. W. *Catal. Rev.* **1973**, *8*, 159. (b) Vlasenko, V. M.; Yuzefovich, G. E. *Russ. Chem. Rev. (Engl. Transl.)* **1969**, *38*, 728. (c) Karn, F. S.; Shultz, J. F.; Anderson, R. B. *Ind. Eng. Chem. Prod. Res. Dev.* **1965**, *4*, 265. (d) Lunde, P. J.; Kester, F. L. *J. Catal.* **1973**, *30*, 423. (e) Gupta, N. M.; Kamble, V. S.; Rao, K. A.; Iyer, R. M. *J. Catal.* **1979**, *60*, 57. (f) Solymosi, F.; Erdöhelyi *J. Mol. Catal.* **1980**, *8*, 471. (g) Zağli, E.; Falconer, J. L. *J. Catal.* **1981**, *69*, 1. (h) Solymosi, F.; Erdöhelyi, A.; Kocsis, M. *J. Chem. Soc., Faraday Trans. 1* **1981**, *77*, 1003. (i) Solymosi, F.; Erdöhelyi, A.; Bánsági, T. *J. Chem. Soc., Faraday Trans. 1* **1981**, *77*, 2645. (j) Ferkul, H. E.; Stanton, D. J.; McCowan, J. D.; Baird, M. C. *J. Chem. Soc., Chem. Commun.* **1982**, 955. (k) Ferkul, H. E.; Berlie, J. M.; Stanton, D. J.; McCowan, J. D.; Baird, M. C. *Can. J. Chem.* **1983**, *61*, 1306. (l) Weatherbee, G. D.; Bartholomew, C. H. *J. Catal.* **1984**, *87*, 352. (m) Darensbourg, D. J.; Ovalles, C. *Inorg. Chem.* **1986**, *25*, 1603.

(3) (a) Vannice, M. A. *J. Catal.* **1975**, *37*, 449. (b) King, D. L. *J. Catal.* **1978**, *51*, 386. (c) Everson, R. C.; Woodburn, E. T.; Kirk, A. R. M. *J. Catal.* **1978**, *53*, 186. (d) Ekerdt, J. G.; Bell, A. T. *J. Catal.* **1979**, *58*, 170. (e) Vannice, M. A.; Garten, R. L. *J. Catal.* **1980**, *63*, 255. (f) Kobori, Y.; Yamasaki, H.; Naito, S.; Onishi, T.; Tamaru, K. *J. Chem. Soc., Faraday Trans. 1* **1982**, *78*, 1473. (g) Kellner, C. S.; Bell, A. T. *J. Catal.* **1982**, *75*, 251. (h) Okuhara, T.; Kimura, T.; Kobayashi, K.; Mosono, M.; Yoneda, Y. *Bull. Chem. Soc. Jpn.* **1984**, *57*, 938. (i) Smith, K. J.; Everson, R. C. *J. Catal.* **1986**, *99*, 349.

(4) (a) Kobori, K.; Naito, S.; Onishi, T.; Tamaru, K. *J. Chem. Soc., Chem. Commun.* **1981**, 92. (b) Okuhara, T.; Kobayashi, K.; Kimura, T.; Misono, M.; Yoneda, Y. *J. Chem. Soc., Chem. Commun.* **1981**, 1114. (c) Kellner, C. S.; Bell, A. T. *J. Catal.* **1981**, *70*, 418. (d) Pierantozzi, R.; Valagene, E. G.; Nordquist, A. F.; Dyer, P. N. *J. Mol. Catal.* **1983**, *21*, 189. (e) Okuhara, T.; Enomoto, T.; Tamaru, H.; Misono, M. *Chem. Lett.* **1984**, 1491. (f) Doi, Y.; Miyake, H.; Yokota, A.; Soga, K. *J. Catal.* **1985**, *95*, 293. (g) Okuhara, T.; Tamaru, H.; Misono, M. *J. Catal.* **1985**, *95*, 41. (h) Jackson, S. D.; Moyes, R. B.; Wells, P. B.; Whyman, R. *J. Chem. Soc., Faraday Trans. 1* **1987**, *83*, 905.

(5) (a) Nijs, H. H.; Jacobs, P. A.; Uytterhoeven, J. B. *J. Chem. Soc., Chem. Commun.* **1979**, 180. (b) Nijs, H. H.; Jacobs, P. A.; Uytterhoeven, J. B. *J. Chem. Soc., Chem. Commun.* **1979**, 1095. (c) Elliott, D. J.; Lunsford, J. H. *J. Catal.* **1979**, *57*, 11. (d) Nijs, H. H.; Jacobs, P. A. *J. Catal.* **1980**, *66*, 401. (e) Ballivet-Tkatchenko, D.; Tkatchenko, I. *J. Mol. Catal.* **1981**, *13*, 1. (f) Blackmond, D. G.; Goodwin, J. G. *J. Chem. Soc., Chem. Commun.* **1981**, 125. (g) Gustafson, B. L.; Lunsford, J. H. *J. Catal.* **1982**, *74*, 393. (h) Leith, I. R. *J. Chem. Soc., Chem. Commun.* **1983**, 93. (i) Okuda, O.; Tatsumi, T.; Fujimoto, K.; Tominaga, H. *Chem. Lett.* **1983**, 1153. (j) Chen, Y. W.; Wang, H. T.; Goodwin, J. G.; Shiflett, W. K. *Appl. Catal.* **1983**, *8*, 303. (k) Chen, Y. W.; Wang, H. T.; Goodwin, J. G. *J. Catal.* **1983**, *83*, 415. (l) Audier, M.; Klinowski, J.; Benfield, R. E. *J. Chem. Soc., Chem. Commun.* **1984**, 626. (m) Wakui, T.; Handa, T. *J. Chem. Soc., Chem. Commun.* **1984**, 994. (n) Chen, Y. W.; Wang, H. T.; Goodwin, J. G. *J. Catal.* **1984**, *85*, 499. (o) Tatsumi, T.; Odajima, H.; Tominaga, H. *J. Chem. Soc., Chem. Commun.* **1985**, 207. (p) Leith, I. R. *J. Catal.* **1985**, *91*, 283. (q) Oukaci, R.; Sayari, A.; Goodwin, J. G. *J. Catal.* **1987**, *106*, 318.

0020-1669/88/1327-3024$01.50/0